PROCEEDINGS OF SCIENCE

# Investigating the Low State of NGC 1275 with VERITAS and *Fermi*-LAT Observations

**Anjana Kaushik Talluri**[a,b,*] **for the VERITAS Collaboration**

[a] *School of Physics & Astronomy, 116 Church St SE, Minneapolis, USA*
[b] *Minnesota Institute for Astrophysics, 116 Church St SE, Minneapolis, USA*

*E-mail:* telid001@umn.edu

The VERITAS observatory is a ground-based imaging atmospheric Cherenkov telescope array that detects very-high-energy (VHE; E>100 GeV) gamma-ray emission from a range of astrophysical sources including more than ~40 Active Galactic Nuclei (AGN). Very few radio galaxies, AGN with relativistic jets oriented at angles offset to our line-of-sight, are detected at VHE including NGC 1275 (3C 84), the central galaxy in the Perseus cluster (z~0.0176). NGC 1275 has a long history of observations across all wavebands, and a complex morphology that has evolved with time. The origin of the TeV emission in NGC 1275 in both the flaring and non-flaring states is still not entirely understood. A VERITAS study of a January 2017 flare finds that a multi-component model is required to fit the multi-wavelength spectral energy distribution (SED). In this study, we present the EBL-corrected, Compton SED peak in the non-flaring state of NGC 1275 constructed with simultaneous VERITAS and *Fermi*-LAT observations over the period 2012-2017.

38th International Cosmic Ray Conference (ICRC2023)
26 July - 3 August, 2023
Nagoya, Japan

*Speaker





PoS(ICRC2023)661

## 1. Introduction

At Very High Energies (VHE; E>100 GeV), the dominant extragalactic sources are blazars–active galactic nuclei (AGN) with relativistic plasma jets oriented very near to our line-of-sight [1]. In contrast, 'radio galaxies' (RGs) have jets oriented at larger viewing angles and therefore due to decreased Doppler boosting, only a handful of nearby RGs have been detected at VHE, including NGC 1275 [2, 3], Cen A [4], M 87 [5], and 3C 264 [6]. The decreased Doppler boosting also enforces a VHE detection bias to nearby RGs which allows the kpc-scale jet to be resolved in high-resolution imaging at lower wavelengths. Coordinated multi-wavelength and VHE observations of RGs enable us to probe the sites of gamma-ray emission and better understand the physical mechanisms involved [7, 8].

As with blazars, the broadband spectral energy distribution (SED) of the jet component in RGs is typically characterized by two peaks: the lower-frequency peak ($10^{12}$ – $10^{15}$ Hz) arises from synchrotron emission, and the higher-frequency (X-ray to TeV) peak is thought most likely to arise from inverse-Compton (IC) upscattering of different seed photon populations by the relativistic electrons in the jet. These can include the optical/UV synchrotron photons themselves (Synchrotron self-Compton or SSC), or photons from the surrounding regions in the AGN or from the ambient Cosmic Microwave Background (CMB) radiation (external inverse-Compton or EIC).

There is a substantial body of research focused on the bright, flaring states of blazars [9–11], which can be easier to detect in VHE due to their high flux states. In comparison, jetted AGN in their low flux states require longer integration times to obtain enough photons for a detection: baseline states, therefore, are less well understood. This is particularly true for the few RGs detected in VHE.

Nonetheless, we need to characterize both flux states to truly understand the underlying mechanisms in these objects and any evolution between states. In particular, the Compton peak is critical for better understanding the particle acceleration mechanisms and the overall energy of the system. In this study, we construct the Compton SED peak in the low state of NGC 1275 with simultaneous High Energy (HE; E>100 MeV) gamma-ray observations from *Fermi*-LAT and VHE gamma-ray observations from VERITAS over the period 2012-2017.

## 2. NGC 1275

Located in the Perseus cluster, NGC 1275 (3C 84; R.A.= $3^{h}\,19^{m}\,48^{s}$, decl.= $41^{\circ}\,30'\,42''$; J2000.0) has a long history of observations across all wavebands and a very complex morphology that has evolved with time. Extensive VLBI observations show an asymmetric jet/counter-jet structure as well as C3, a component associated with a radio outburst that started in 2005 [12]. There was an initial brightening of C3 followed by a breakout phase around the time of a gamma-ray flare in 2017, with C3 dimming significantly by 2020 [13]. Previous studies suggested that the parsec scale environment, where C3 is situated, is likely suffused with either clumpy clouds or dense ionized gas leading to possible interaction between the jet and the clouds or gas [13, 14].

Both MAGIC [Major Atmospheric Gamma Imaging Cherenkov; 2] and VERITAS [Very Energetic Radiation Imaging Telescope Array System; 3] telescopes have reported several significant detections of NGC 1275 in the VHE band [2, 15–17]. In January 2017, MAGIC detected an extraordinary flare at TeV energies in NGC 1275. The brightest outburst was around 1.5 times the flux from the Crab nebula (C.U.) above 100 GeV [18, 19]. Intriguingly, Swift-XRT data show an

"orphan" flare several days after the VHE flare. An ensuing study by VERITAS, including MAGIC published data, over the two days of the VHE flare found that a multi-zone SSC model (with two SSC components) and a strong EIC component were required to fit the MWL SED assuming an 18° angle between the jet and line of sight [20].

Recently, another VHE flare was observed from NGC 1275 on the night of December 21, 2022 UTC by LST-1 and MAGIC [21, 22] and followed up by VERITAS. LST-1 reported that the peak of the flux reached about 140% Crab [22]. Unlike the 2017 flare which had a decay time of hours [19], the 2022 flare is characterized by multiple flaring events over the course of the month reaching again about 100% Crab in early January. Preliminary VERITAS analysis of a 30 min exposure on December 21st covering part of the 2022 flare returns a significance of $\sim 14\sigma$ and an integral flux: I(>200 GeV) = $(1.7 \pm 0.3) \times 10^{-10}$ cm$^{-2}$ s$^{-1}$ which corresponds to $\sim$ 80% C.U. above the same threshold [23]. The full dataset for VERITAS remains to be analyzed.

## 3. The VERITAS Instrument

VERITAS [24, 25] is an array of Imaging Atmospheric Cherenkov Telescopes at the Fred Lawrence Whipple Observatory in Arizona. It is sensitive to photons from $\sim$ 100 GeV to $\sim$30 TeV and consists of four telescopes separated by $\sim$ 100m. Each of the telescopes is based on the Davies-Cotton optical design and has a large reflector of diameter 12m made of 345 hexagonal mirror facets. Incoming Cherenkov light is reflected onto a camera with 499 photomultiplier tubes (PMTs). VERITAS has an energy resolution of $\sim$15% at 1 TeV and a sensitivity to a 1% Crab Nebula flux source in < 25h.

## 4. Observations and Low State Selection

To investigate the Compton peak of the low state of NGC 1275, we must select low-state data that is simultaneous in both Fermi-LAT and VERITAS instruments. The low state of NGC 1275 in the gamma-ray band was defined with the following strategy:

1. Light curves were constructed for *Fermi*-LAT and VERITAS observations between 2012-2017.
2. A threshold was set to identify any flares within each band. Any potential high states were removed, and the baseline state was selected for each band as outlined in sections 4.1 and 4.2 below.
3. Time constraints were applied to the HE and VHE datasets to ensure as much simultaneity between the bands as possible.
4. When a flare was identified in one band, simultaneous data were removed from the other band as well.

### 4.1 *Fermi*-LAT

*Fermi*-LAT observations were obtained between 0.1 GeV and 300 GeV over the period 2012 through 2017. We used the 4FGL *Fermi*-LAT source catalog [26] and obtained all point sources within a region of radius of 25° centered on NGC 1275 (4FGL J0319.8+4130). We utilized the open source python package `Fermipy v1.2` for the analysis [27], along with Galactic (`gll_iem_v07.fits`) and isotropic diffuse (`iso_P8R3_SOURCE_V3_v1.txt`) templates for the background model. We used a zenith angle cut of 90° to reduce contamination from Earth limb gamma-rays. To check for the variability in flux, we plotted the long-term *Fermi*-LAT lightcurve over 2012-2017 (which included flares) in bin sizes of one month.

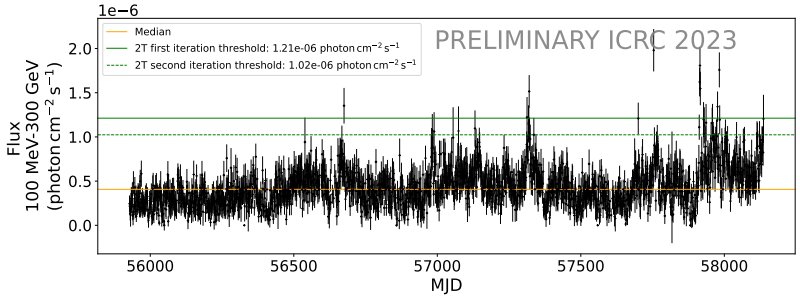


**Figure 1:** Monthly binned *Fermi*-LAT lightcurve over the period 2012 to 2017. The median of the data is shown in yellow. The 2T thresholds calculated with MAD (see text) are shown in green. The flux threshold for the first iteration to identify the most significant flares (solid green line) is $1.21\times10^{-6}$ photon cm$^{-2}$ s$^{-1}$ and that for the second iteration to identify potential high states (dashed green line) is $1.02\times10^{-6}$ photon cm$^{-2}$ s$^{-1}$.

As the data displayed variability, we applied the Two-Stage Thresholding (2T) technique outlined in [28] for the selection of flares. Specifically, we applied Equations 2 and 3 from [28] to determine the Median Absolute Deviation (MAD), and any data greater than three MADs away from the median was considered to be a flare and was removed. Two such iterations of flare-finding and data removal were performed to obtain the low state in the HE band. Figure 1 shows the monthly binned *Fermi*-LAT data in black and the median of the data in yellow. The flux thresholds for the first and second iterations of the 2T technique with MAD are indicated by the solid and dashed green lines respectively; the first iteration identifies the most significant flares and the second iteration identifies the high states in the HE band.

### 4.2 VERITAS

Long term observations of NGC 1275 from 2012 to 2017 are used to determine a low state by removing flux points in the daily binned light curve corresponding to the extreme flare states in January 2017 and high states corresponding to other flares. Flares are defined to be any data more than three standard deviations away from the mean, and two iterations of flare-finding and data removal were performed to obtain a low state in VHE [20]. VERITAS data were analyzed with two independent analysis packages [29, 30] and were found to yield consistent results; we employed an Image Template Method (ITM) in our analysis for improved event reconstruction [31]. The total exposure of the low state data was ~53 h and the significance was $\sim12\sigma$. The VERITAS light curve corresponding to Figure 1 will be published in [20].

## 5. Results: Fitting of the Compton Peak

A low state Compton peak is constructed with simultaneous *Fermi*-LAT and VERITAS data. The data are fit to four spectral models using the `gammapy` package [32, 33]. Firstly, we fit a simple power law (PL) model

$$\frac{dN}{dE} = k_0 \left(\frac{E}{E_0}\right)^{-\gamma} \tag{1}$$

where $k_0$ is the normalization factor in units of cm$^{-2}$ s$^{-1}$ TeV$^{-1}$, $\gamma$ is the photon spectral index, and $E_0$ is the pivot energy in units of TeV. Secondly, we fit a log parabola (LP) model

$$\frac{dN}{dE} = k_0 \left(\frac{E}{E_0}\right)^{-\alpha-\beta\log(E/E_0)} \tag{2}$$

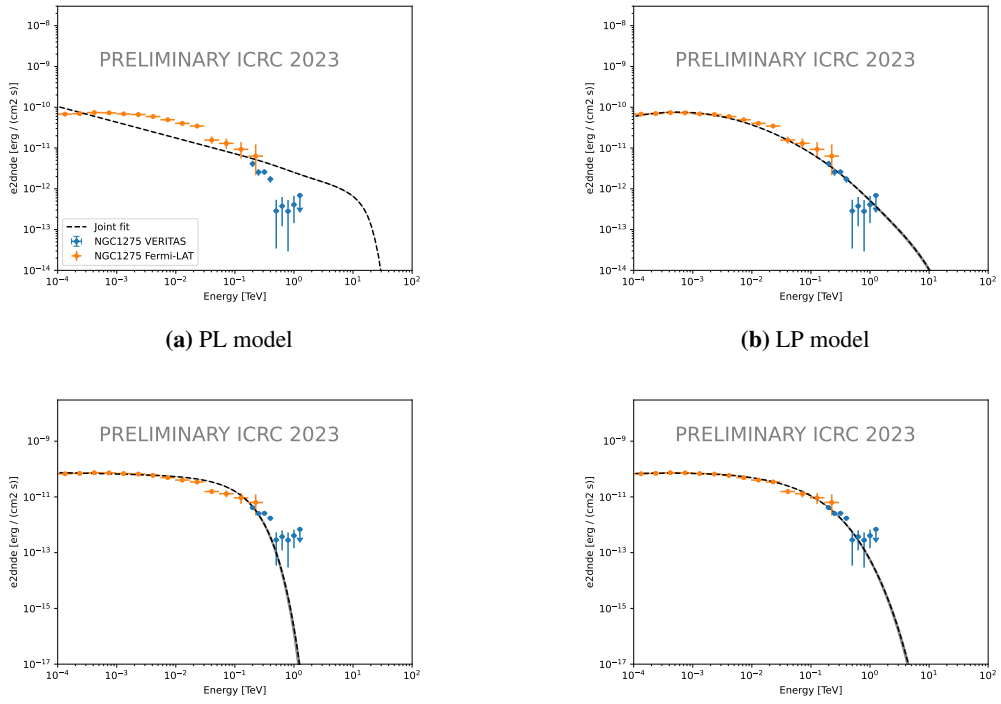


**(a)** PL model

**(b)** LP model

**(c)** ECPL model

**(d)** Sub-ECPL model

**Figure 2:** Panel of images showing the low state Compton SED peak constructed with both *Fermi*-LAT and VERITAS observations over 2012-2017. The data are fit with four spectral models which are corrected for EBL attenuation: a PL in (a), a LP in (b) and an ECPL in (c) and a sub-ECPL in (d). Based on the total stat parameter (shown in Table 1), we find that there is significance curvature in the spectrum.

where $\alpha$ is the index, $\beta$ is the curvature, and $E_0$ is the pivot energy. Finally, we fit the power-law with exponential cutoff (ECPL) and the power-law with sub-exponential cutoff (sub-ECPL) models

$$\frac{dN}{dE} = k_0 \left(\frac{E}{E_0}\right)^{-\Gamma} exp(-(\lambda E)^{\alpha}) \tag{3}$$

where $\Gamma$ is the power-law index, $\lambda$ is the inverse of the cutoff energy in TeV, and $E_0$ is the pivot energy. The parameter $\alpha$ (exponential index) is the cutoff strength and is equal to 1 for ECPL and 0.5 for sub-ECPL models respectively.

The Compton SED needs to be corrected for absorption by the Extragalactic Background Light (EBL), which depends on both the gamma-ray energy and source distance. We adopted the Franceschini model [34] and applied an appropriate EBL correction to each of these spectral models. Figure 2 shows the low state Compton SED peak fit with each of the above four spectral models corrected for EBL absorption– PL in (a), LP in (b), ECPL in (c) and sub-ECPL in (d). The best fitting model parameters for each spectral model are listed in Table 1. The 'total stat' parameter is returned by `gammapy` and indicates two times the negative log-likelihood value for each fit.

To test whether the spectrum can be best described by a power law or requires some curvature, we estimate the Test Statistic (TS = $2 \times (\log L_{\rm curved} - \log L_{\rm PL})$) where $L_{\rm curved}$ represents either the LP, ECPL or sub-ECPL log-likelihood values. A TS>16 indicates that the spectrum is significantly

| **Model** | **Parameter** | **Best fit value** |
|---|---|---|
| Power Law | $\gamma$ | 2.4 ± 0.003 |
| | $E_0$ [TeV] | 1 (fixed) |
| (Total stat =3210) | $k_0$ [$cm^{-2}$ $s^{-1}$ $TeV^{-1}$] | 1.86e-12 ± 5e-14 |
| Log Parabola | $\alpha$ | 3.3 ± 0.03 |
| | $\beta$ | 0.086 ± 0.002 |
| (Total stat =87) | $E_0$ [TeV] | 1 (fixed) |
| (AIC estimate=93) | $k_0$ [$cm^{-2}$ $s^{-1}$ $TeV^{-1}$] | 3.7e-13 ± 3e-14 |
| Power Law Exp Cutoff | $\Gamma$ | 2.05 ± 0.006 |
| | $\alpha$ | 1 (fixed) |
| | $E_0$ [TeV] | 1 (fixed) |
| (Total stat =193) | $\lambda$ [$TeV^{-1}$] | 12 ± 0.7 |
| (AIC estimate=199) | $k_0$ [$cm^{-2}$ $s^{-1}$ $TeV^{-1}$] | 3.04e-11 ± 1e-12 |
| Power Law sub-Exp Cutoff | $\Gamma$ | 1.93 ± 0.009 |
| | $\alpha$ | 0.5 (fixed) |
| | $E_0$ [TeV] | 1 (fixed) |
| (Total stat =45) | $\lambda$ [$TeV^{-1}$] | 59.7 ± 4.1 |
| (AIC estimate=51) | $k_0$ [$cm^{-2}$ $s^{-1}$ $TeV^{-1}$] | 9.35e-11 ± 7e-12 |

**Table 1:** Best fitting parameters of the joint spectral fit of *Fermi*-LAT and VERITAS gamma-ray data. The first row shows the result of the PL fit, the second row shows the LP fit, the third row shows the ECPL fit, and the last row shows the sub-ECPL fit parameters. Twice the negative log-likelihood value for each fit is indicated by the 'total stat' parameter. The sub-ECPL has the lowest AIC estimate and is favored over the other curved models.

curved [35]. We find that LP, ECPL, and sub-ECPL represent the Compton peak better than the PL with significances of $\sqrt{\text{TS}} \sim 56\sigma$, $\sqrt{\text{TS}} \sim 55\sigma$ and $\sqrt{\text{TS}} \sim 56\sigma$ respectively, indicating that the spectrum is significantly curved.

To determine the best curvature model, we apply the Akaike Information Criterion (AIC) test: AIC = $2k - 2\ln(L)$ where L is the likelihood and k is the number of free parameters; the model with the lowest AIC is favored. The AIC estimates for the three curved models are included in Table 1. We find that the sub-ECPL with a cutoff energy of 16 GeV is the best representation of the low state data when compared to the LP and ECPL models.

A possible interpretation of a sub-exponential photon spectrum is: an electron energy distribution of a power law with an exponential cutoff [36] which may arise from Fermi acceleration at a collisionless shock in the Thomson regime; when energy losses dominate, there is an exponential decrease in the number of particles, and this deviates the spectral shape from a power law to a power law with an exponential cutoff. However, the curvature may also arise from absorption or Klein-Nishina effects, and this will be further investigated with the full SED in our upcoming paper.

## 6. Conclusion

NGC 1275 is one of the brightest, compact radio sources and is known to emit radiation ranging from radio to VHE gamma-rays. The physical mechanisms responsible for the high-level VHE emission observed are still unclear. Additional insight may be gained on the origin of VHE gamma-rays through an in-depth study of the source in both its flaring and non-flaring states.

In this work, we present a low state Compton SED peak of NGC 1275 made with simultaneous *Fermi*-LAT and VERITAS observations over the years 2012-2017. We fit the Compton peak to four spectral models and find that the curved models (LP, ECPL and sub-ECPL) are better representations of the data when compared to a simple PL model. In addition, we apply the AIC to compare the

curved spectral models. We find that sub-ECPL model ($\alpha$ = 0.5) with a cutoff energy at 16 GeV is favored over other models.

A possible interpretation of a sub-ECPL photon spectrum may be an electron energy distribution of a power law with an exponential cutoff [36] which may arise from Fermi acceleration at a collisionless shock. In the future, a comparison of the quiescent state results with those from the December 2022-January 2023 flare may provide us with a deeper insight into any spectral evolution across both states. To probe the origin of gamma-rays in NGC 1275, we plan to extend our study by constructing contemporaneous multi-wavelength SEDs in both the low state and the recent flare state with observations from ALMA, Swift-UVOT, Swift-XRT, and NuSTAR telescopes.

## Acknowledgements

This research was partially supported by the National Science Foundation under grants PHY 2110737 and DGE-1922512. This research is supported by grants from the U.S. Department of Energy Office of Science, the U.S. National Science Foundation and the Smithsonian Institution, by NSERC in Canada, and by the Helmholtz Association in Germany. This research used resources provided by the Open Science Grid, which is supported by the National Science Foundation and the U.S. Department of Energy's Office of Science, and resources of the National Energy Research Scientific Computing Center (NERSC), a U.S. Department of Energy Office of Science User Facility operated under Contract No. DE-AC02-05CH11231. We acknowledge the excellent work of the technical support staff at the Fred Lawrence Whipple Observatory and at the collaborating institutions in the construction and operation of the instrument.

## References

[1] Rieger, F.M. Galaxies 2019, 7, 28

[2] Aleksic, J., Alvarez, E. A., Antonelli, L. A., et al. 2012, A&A, 539, L2, doi: 10.1051/0004-6361/2011186

[3] Mukherjee, R., & VERITAS Collaboration. 2017, The Astronomer's Telegram, 9931, 1

[4] Acciari, V. A., Beilicke, M., Blaylock, G., et al. 2008, The Astrophysical Journal, 679, 397

[5] Abramowski, A., Acero, F., Aharonian, F., et al. 2012, ApJ, 746, 151

[6] Archer, A., Benbow, W., Bird, R., et al. 2020, ApJ, 896

[7] Hodgson J. A., et al., 2021, ApJ, 914, 43

[8] Roychowdhury, A., Meyer, E.T., Georganopoulos, M., et al. 2022, , 924, 57

[9] F. Aharonian et al 2007 ApJ 664 L71

[10] A. U. Abeysekara et al 2015 ApJ 815 2

[11] A. U. Abeysekara et al 2020 ApJ 890 97

[12] Nagai, H., Suzuki, K., Asada, K., et al. 2010, PASJ, 62, L11

[13] Motoki Kino et al 2021 ApJL 920 L24

[14] Wajima K., Kino M., Kawakatu N., 2020, ApJ, 895, 35

[15] Benbow W., VERITAS Collaboration 2015, in 34th International Cosmic Ray Conference (ICRC2015). p. 821

[16] Mukherjee R., VERITAS Collaboration 2016, The Astronomer's Telegram, 9690, 1

[17] Mirzoyan R., 2016, The Astronomer's Telegram, 9689, 1

[18] Mirzoyan, R. 2017, The Astronomer's Telegram, 9

[19] MAGIC Collaboration, A&A 617, A91 (2018)

[20] Rulten et al. in prep

[21] Blanch O., Nievas Rosillo M., Arbet-Engels A., Nigro C., Molero M., 2022, ATel, 15820

[22] Cortina & CTA LST Collaboration, 2022, ATel, 15819

[23] F. Aharonian et al., 2010 A&A 521, A69

[24] Weekes, T. C., Badran, H., Biller, S. D., et al. 2002, Astroparticle Physics, 17, 221

[25] Holder, J., Atkins, R. W., Badran, H. M., et al. 2006, Astroparticle Physics, 25, 39

[26] Abdollahi, S., Acero, F., Ackermann, M., et al. 2020, The Astrophysical Journal Supplement Series, 247, 33

[27] Wood, M., Caputo, R., Charles, E., et al. 2021, 301, 824

[28] AIIPCC '19: Proceedings of the International Conference on Artificial Intelligence, Information Processing and Cloud ComputingDecember 2019Article No.: 37

[29] Cogan, P. 2008, in Proceedings of the 30th International Cosmic Ray Conference, ICRC 2007, Vol. 3, 1385–1388

[30] Maier, G., Holder, J. 2017, in 35th International Cosmic Ray Conference (ICRC2017), Vol. 301, Proceedings of Science (Sissa Medialab Srl), 747

[31] Christiansen, J. 2017, PoS, ICRC2017, 789, doi: 10.22323/1.301.0789

[32] C. Deil, R. Zanin, J. Lefaucheur, et al., 35th International Cosmic Ray Conference (ICRC2017), volume 301 of International Cosmic Ray Conference, 2017, p. 766

[33] Deil, C., Donath, A., Terrier, R., et al. 2021, gammapy/gammapy: v0.19, 10.5281/zenodo.5721467

[34] Franceschini A et al. 2008 A&A. 487:837

[35] Acero F., et al., 2015, ApJS, 218, 23

[36] V. A. Acciari et al 2009 ApJ 706 L275

## Full Author List: VERITAS Collaboration

A. Acharyya[1], C. B. Adams[2], A. Archer[3], P. Bangale[4], J. T. Bartkoske[5], P. Batista[6], W. Benbow[7], J. L. Christiansen[8], A. J. Chromey[7], A. Duerr[5], M. Errando[9], Q. Feng[7], G. M. Foote[4], L. Fortson[10], A. Furniss[11,12], C. Hahn[13], W. Hanlon[7], O. Hervet[12], C. E. Hinrichs[7,14], J. Hoang[12], J. Holder[4], Z. Hughes[9], T. B. Humensky[15,16], W. Jin[1], M. N. Johnson[12], M. Kertzman[3], M. Kherlakian[6], D. Kieda[5], T. K. Kleiner[6], N. Korzoun[4], S. Kumar[15], M. J. Lang[17], M. Lundy[18], G. Maier[6], C. E McGrath[19], E. T. Meyer[13], M. J. Millard[20], C. L. Mooney[4], P. Moriarty[17], R. Mukherjee[21], S. O'Brien[18,22], R. A. Ong[23], N. Park[24], C. Poggemann[8], M. Pohl[25,6], E. Pueschel[6], J. Quinn[19], P. L. Rabinowitz[9], K. Ragan[18], P. T. Reynolds[26], D. Ribeiro[10], E. Roache[7], J. L. Ryan[23], I. Sadeh[6], A. C. Sadun[27], L. Saha[7], M. Santander[1], G. H. Sembroski[28], R. Shang[21], M. Splettstoesser[12], A. K. Talluri[10], J. V. Tucci[29], V. V. Vassiliev[23], A. Weinstein[30], D. A. Williams[12], S. L. Wong[18], and J. Woo[31]

[1]Department of Physics and Astronomy, University of Alabama, Tuscaloosa, AL 35487, USA
[2]Physics Department, Columbia University, New York, NY 10027, USA
[3]Department of Physics and Astronomy, DePauw University, Greencastle, IN 46135-0037, USA
[4]Department of Physics and Astronomy and the Bartol Research Institute, University of Delaware, Newark, DE 19716, USA
[5]Department of Physics and Astronomy, University of Utah, Salt Lake City, UT 84112, USA
[6]DESY, Platanenallee 6, 15738 Zeuthen, Germany
[7]Center for Astrophysics | Harvard & Smithsonian, Cambridge, MA 02138, USA
[8]Physics Department, California Polytechnic State University, San Luis Obispo, CA 94307, USA
[9]Department of Physics, Washington University, St. Louis, MO 63130, USA
[10]School of Physics and Astronomy, University of Minnesota, Minneapolis, MN 55455, USA
[11]Department of Physics, California State University - East Bay, Hayward, CA 94542, USA
[12]Santa Cruz Institute for Particle Physics and Department of Physics, University of California, Santa Cruz, CA 95064, USA
[13]Department of Physics, University of Maryland Baltimore County, 1000 Hilltop Circle, Baltimore, MD 21250, USA
[14]Department of Physics and Astronomy, Dartmouth College, 6127 Wilder Laboratory, Hanover, NH 03755 USA
[15]Department of Physics, University of Maryland, College Park, MD, USA
[16]NASA GSFC, Greenbelt, MD 20771, USA
[17]School of Natural Sciences, University of Galway, University Road, Galway, H91 TK33, Ireland
[18]Physics Department, McGill University, Montreal, QC H3A 2T8, Canada
[19]School of Physics, University College Dublin, Belfield, Dublin 4, Ireland
[20]Department of Physics and Astronomy, University of Iowa, Van Allen Hall, Iowa City, IA 52242, USA
[21]Department of Physics and Astronomy, Barnard College, Columbia University, NY 10027, USA
[22] Arthur B. McDonald Canadian Astroparticle Physics Research Institute, 64 Bader Lane, Queen's University, Kingston, ON Canada, K7L 3N6
[23]Department of Physics and Astronomy, University of California, Los Angeles, CA 90095, USA
[24]Department of Physics, Engineering Physics and Astronomy, Queen's University, Kingston, ON K7L 3N6, Canada
[25]Institute of Physics and Astronomy, University of Potsdam, 14476 Potsdam-Golm, Germany
[26]Department of Physical Sciences, Munster Technological University, Bishopstown, Cork, T12 P928, Ireland
[27]Department of Physics, University of Colorado Denver, Denver, Colorado, CO 80217, USA
[28]Department of Physics and Astronomy, Purdue University, West Lafayette, IN 47907, USA
[29]Department of Physics, Indiana University-Purdue University Indianapolis, Indianapolis, IN 46202, USA
[30]Department of Physics and Astronomy, Iowa State University, Ames, IA 50011, USA
[31]Columbia Astrophysics Laboratory, Columbia University, New York, NY 10027, USA